PHOTONIC MATERIALS

Monomer-biased manufacture of industrial-scale colloidal photonic films

Huateng Li[1], Junying Yang[1,2], Guowei Zhao[1], Hanwen Huang[1], Lulu Chen[1], Ruoqi Lan[1], Feng Tian[3], Weihua Li[1], Jade A. McCune[4], Oren A. Scherman[4]*, Changchun Wang[1]*

Complex functions in nature arise from the ordered assembly of simple building blocks. Transformation of colloidal aggregates into industrial-scale photonic crystals under rapid ambient conditions remains challenging owing to high energy barriers and limited assembly control. In this study, common monomers act as mediators that lower these barriers and bias ambient shear-induced ordering within seconds. This enables in situ processing compatible with roll-to-roll manufacturing of colloidal photonic crystal films with tunable mechanical properties. Robust 15-micrometer-thick films, incorporating a supramolecular matrix, can be produced up to 4000 meters long and 1.3 meters wide at a rate of 25 meters per minute. These combine vivid structural color and high transparency (>90%) with mechanical robustness and rapid self-healing, demonstrating a scalable route to high-quality colloidal photonic materials.

The spontaneous assembly from disordered systems into highly ordered structures is typically considered slow and highly energetically unfavorable (*1*–*5*), especially under ambient conditions. For example, biological functions typically emerge through slow developmental processes (*6*), and the formation of defect-free colloidal crystals usually demands prolonged assembly times (*7*). Such processes are inherently hindered by substantial entropic penalties, high energy barriers, and a delicate balance of interactions (*8*–*10*). Consequently, enabling rapid, robust, and manufacturable disorder-to-order assembly at room temperature remains a considerable challenge.

Biological systems have evolved efficient strategies to rapidly construct functional ordered structures. For example, diatoms use positively charged polyamines to precisely regulate the rapid condensation and assembly of silica precursors into nanoscale ordered architectures while embedding these small molecules within the structure to enhance mechanical stability (*11*). Similarly, spider silk proteins, with the assistance of ionic gradients, undergo rapid alignment into β-sheet–rich crystalline domains under shear forces. Followed by in situ solidification, the fibers show exceptional strength and toughness (*12*). Despite differences in composition and morphology, these systems share a common principle: Molecular mediators bias assembly pathways to create a useful formulation and open an effective processing window, enabling rapid ordering and reinforcing structural stability through molecular incorporation (*13*, *14*).

Inspired by these biological systems, we developed a monomer-mediated strategy for colloidal assembly. Low-molecular-weight functional monomers bias the assembly pathway of colloidal particles, enabling rapid ordering under ambient and template-free conditions. Subsequent in situ polymerization locks the colloidal particles within a robust matrix, where dual-network interactions, enabled by supramolecular chemical design, impart macroscopic structural stability and mechanical robustness. The resulting materials exhibit tunable photonic bandgaps (PBGs), displaying vivid structural color.

[1]State Key Laboratory of Molecular Engineering of Polymers, Department of Macromolecular Science, and Laboratory of Advanced Materials, Fudan University, Shanghai, China. [2]Department of Physics, Wenzhou University, Wenzhou, Zhejiang, China. [3]Phomera Metamaterials, Zhuhai, Guangdong, China. [4]Melville Laboratory for Polymer Synthesis, Yusuf Hamied Department of Chemistry, University of Cambridge, Cambridge, UK. ***Corresponding author. Email: ccwang@fudan.edu.cn (C.W.); oas23@cam.ac.uk (O.A.S.)**

Overview and mechanism of monomer-biased colloidal assembly

The fabrication of colloidal photonic crystal (CPC) films, through disorder-to-order colloidal particle transitions, is a process driven by a range of external forces (capillary, shear, and evaporation) (*15*), in which the magnitude of the driving force determines the assembly efficiency and interactions among the colloidal particles govern the assembly quality. In conventional evaporation-induced self-assembly (*16*–*19*), the interactions between colloidal particles can be tuned, enabling the preparation of three-dimensional (3D) CPCs with excellent optical and mechanical properties. However, the inherently weak driving force substantially limits the assembly efficiency (*20*). Shear-induced assembly provides a stronger driving force, substantially improving the assembly rate; however, liquid colloidal systems often need annealing to reach ordered states (*21*, *22*), and polymer-melt systems usually depend on elevated temperatures and weaker particle interactions (*23*, *24*), resulting in materials with compromised mechanical properties and structural stability (*25*). Therefore, considering the imbalance between the tunability of interparticle interactions and the magnitude of driving forces, fabrication of industrial-scale CPC films typically sacrifices at least one factor: assembly rate, optical performance, or mechanical properties, forming a triangular trade-off (fig. S1) (*26*, *27*).

Core-shell microspheres (Fig. 1A and figs. S2 to S4) are mixed with mediators (commonly used monomers) (Fig. 1B) that are readily compatible with the colloidal shell. This facilitates the rapid formation of ordered structures upon shear, in which the cores act as the building blocks and the shells fuse together into the matrix (Fig. 1C). In the absence of mediating monomers, well-ordered colloidal structures do not form on a relevant timescale. Systems are often trapped in local free-energy minima and must overcome multiple energy barriers, making it difficult to achieve an ordered structure within a short timescale. When monomers are introduced as mediators, they effectively lower the initial energy state of the system (Fig. 1C, $E_3 < E_1$) and substantially reduce the energy barriers, biasing the rapid organization of particles toward a highly ordered state (*9*, *28*). In this ordered state, an individual colloidal particle possesses greater freedom to vibrate and rotate within its lattice site, further minimizing the overall free energy of the system (Fig. 1C, $E_4 < E_2$). After ordered assembly, monomers in the colloidal shell undergo rapid polymerization upon exposure to ultraviolet (UV) light (365 nm), arresting the particles while yielding a matrix, ensuring mechanical robustness. Reverse nonequilibrium molecular dynamic (RNEMD) simulations (fig. S5 and supplementary text 1) further supported this mechanism: When the interparticle interactions between microspheres are strong, shear fails to induce a highly ordered structure, resembling a colloidal glass (figs. S6, A and B, and S7, A to C). Introducing mediating monomers weakens colloidal interactions, resulting in a highly ordered structure upon shear (figs. S6, C and D, and S7, D and E).

This strategy allows for a broad choice of monomers with Hildebrand solubility parameters in the range of 18.0 to 24.6 because all exhibit facile colloidal assembly regardless of polarity, hydrophilicity or hydrophobicity, or the presence of ionic functional groups. For core-shell microspheres, a monomer content of 25 wt % (minimum amount to form a stable slurry) was sufficient to yield films exhibiting structural color with a well-defined full width at half maximum (FWHM) upon shear (Fig. 1D and fig. S8) in 10 s (fig. S9), which is indicative of highly ordered colloidal packing. To further elucidate the role of the monomer mediators, we systematically investigated core-shell microspheres with

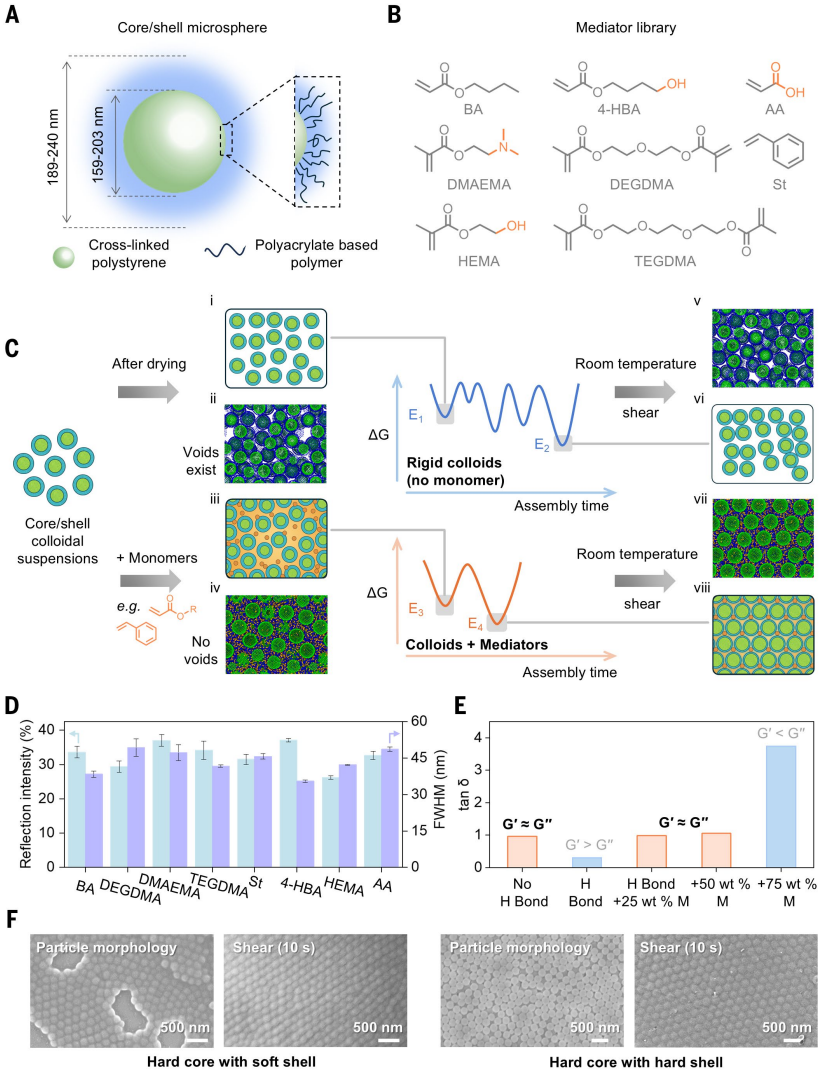

Fig. 1. Overview and mechanism of monomer-biased colloidal assembly. (**A**) Structure and the components of the core-shell microsphere. (**B**) Chemical structures of the mediator library. BA, butyl acrylate; DEGDMA, diethylene glycol dimethacrylate; St, styrene; DMAEMA, (dimethylamino)ethyl methacrylate; TEGDMA, triethylene glycol dimethacrylate; 4-HBA, 4-hydroxybutyl acrylate; HEMA, 2-hydroxyethyl methacrylate; and AA, acrylic acid. (**C**) Schematic illustration of the monomer-biased assembly. Black-outlined images indicate schematic representations of the structures observed in the RNEMD simulations. Green, blue, and yellow beads indicate the cores, shells, and monomers in RNEMD simulations, respectively. (**D**) Reflection intensity and FWHM of CPC with different kinds of mediating monomers (measured at three locations on each sample; error bars indicate mean ± SD). (**E**) Summary of the loss factors (tanδ) of core-shell microspheres with varying compositions at 0.3 Hz storage (G', storage moduli; G'', loss moduli). Measurements conducted at setting strain amplitude (γ) of 100%. (**F**) FESEM images of the original morphology of particles with soft shell (polybutyl acrylate; $T_g = -40$°C) and hard shell (polyisobutyl methacrylate; $T_g = 65$°C), and particle arrangement with mediating monomer upon shear.

hydrogen-bonded (H bond) shells (fig. S10A), non–hydrogen-bonded (no H bond) shells (fig. S10B), and H bond shells with varying monomer content. We summarized and compared the optical characteristics of the assembled systems (fig. S11A). At room temperature, microspheres with soft shells lacking hydrogen bonding could be shear-induced into highly ordered photonic crystal structures, yielding vivid structural color (fig. S11B). By contrast, when the shell contained hydrogen bonds, shear no longer induced ordering, despite the shells remaining soft (fig. S11C). When monomers [such as 4-hydroxybutyl acrylate (4-HBA) and diethylene glycol dimethacrylate (DEGDMA)] were added to colloids with hydrogen bonding present in their shell, vivid structural color was achieved upon shear (fig. S11, D and E). Nevertheless, a critical threshold exists: When the monomer content exceeded 75 wt %, no distinct reflection peak was observed (fig. S11F). Field emission scanning electron microscopy (FESEM) images revealed the arrangement of microspheres in the films; a variation in the level of ordering is consistent with changes in optical properties (fig. S12).

Molecular dynamics (MD) simulations (supplementary text 2) of the polymer chains in the colloidal shell (fig. S13) revealed that the introduction of hydrogen bonds increased the van der Waals (vdW) interaction energy by nearly 15% between chains (from −14,819 to −16,501 kJ/mol). This was accompanied by a reduction in polymer chain mobility, as evidenced by decreased mean square displacement (MSD) (fig. S14A) and diffusion coefficient (from 3.95×10^{-8} to 3.73×10^{-8} cm^2/s). Incorporation of mediating monomers simultaneously increased monomer-polymer interactions, weakened polymer chain-chain interactions, and enhanced polymer chain mobility (figs. S14B and S15). Fourier transform infrared (FTIR) spectra results suggested that the mediating monomer inserted between the shell polymer chains mainly through solvent effects and hydrogen-bonding interactions (fig. S16). On the basis of this trend, we found that shear-induced ordering of colloidal particles occurs only when the intermolecular interactions between polymer chains are appropriately balanced.

The colloidal shells, with different polymer chain mobilities (dependent on the amount of mediating monomer added), exhibited various viscoelastic states at room temperature. We characterized the rheological properties of systems at a fixed strain amplitude of 100%, above yield strain (fig. S17), to better simulate real shear conditions. We summarized representative loss factor (tanδ) of different systems at 0.3 Hz, which revealed the influence of monomer mediators on the viscoelastic behavior of the polymer shell (Fig. 1E). Without hydrogen bonding in the shell, the storage modulus (G') and loss modulus (G'') were similar at low frequencies (fig. S18A), which is indicative of a viscoelastic state. Introducing hydrogen bonding in the shell increased G' over G'' (fig. S18B), shifting the system into an elastic solid state unfavorable for shear-induced assembly. Adding 25 to 50 wt % mediating monomers restored the system to a viscoelastic regime ($G' \approx G''$, tanδ ≈ 1) (fig. S18, C and D), exhibiting both fluidity and elasticity (*29*–*31*), which is optimal for rapid shear-induced colloidal assembly. The fluidity allows the momentum created from external shear forces to be transmitted through the polymer network, mobilizing the microspheres. The elasticity indicates that the system undergoes dynamic recovery of chain entanglements once shear is removed, causing oscillations between microspheres (*32*). Excessive monomer addition (75 wt %) caused G'' to surpass G' (fig. S18E), resulting in the system entering a viscous liquid state. These findings demonstrate that an appropriate amount of mediating monomers can tune the viscoelasticity of the matrix, allowing the system to access a kinetic regime (tanδ ≈ 1) (Fig. 1E) in which rapid crystallization can occur at room temperature (*28*) and controlled access to facile colloidal assembly is enabled. This monomer-mediated approach is not only applicable to both soft- and hard-shell microspheres [we used polyisobutyl methacrylate,

glass transition temperature (T_g) = 65°C, as the hard shell (Fig. 1F)] but can also be applied to polymethyl methacrylate (PMMA), silicon dioxide (SiO_2), and cadmium sulfide (CdS) colloidal particles (fig. S19).

Industrial-scale fabrication of 3D colloidal structural color films

Uniformity of core-shell particles fundamentally determines the optical performance of the fabricated photonic crystal films. Highly uniform core-shell particles were synthesized by means of a semicontinuous seeded emulsion polymerization, enabling the preparation of high-solid-content (47 wt %) colorful colloidal suspensions in a metric ton–scale reactor (figs. S20 and S21). Particle size was finely controlled by adjusting the SDS concentration in the seed stage (table S1), and the morphology of core-shell particles subsequently used to fabricate representative blue, green, and red photonic crystal films are displayed in fig. S4. We developed a customized roll-to-roll industrial coating line (Fig. 2A, fig. S22, and movies S1 and S2) capable of fabricating 3D CPC films at a speed of 25 m/min. The production process comprised coating, drying, shearing, UV curing, and winding. The microscale process during preparation is shown in Fig. 2B. The stable coating solution (fig. S23, movies S3 and S4, and supplementary text 3) was prepared by mixing the core-shell microsphere suspensions with mediating monomers. To ensure that the resulting films exhibited desirable elasticity, toughness, and self-healing properties, we selected 1:1 ratio 4-HBA and DEGDMA as the mediating monomers, added at 25 wt %. When the solution was deposited onto a polyethylene terephthalate (PET) substrate by means of microgravure coating, monomer-adsorbed microspheres maintained their core-shell structures and remained uniformly dispersed in water. Upon water evaporation (figs. S24 and S25 and supplementary text 4), interparticle spacing progressively decreased, and the presence of mediating monomers allowed the system to reach a room-temperature regime conducive to rapid crystallization, with tanδ near 1. Mediating monomers enabled uniform fusion of the microsphere shells into a continuous film with evenly distributed polystyrene (PS) cores, enhancing film wettability and effectively preventing cracks (fig. S26). After laminating into a PET-slurry-PET sandwiched structure, continuous roller bending–induced shear at room temperature facilitated the ordered arrangement of PS microspheres within the polymer matrix, producing vivid structural color. The entire assembly process was carried out at room temperature, and reflectance, transmittance, ultrasmall angle x-ray scattering (USAXS), and FESEM analyses (figs. S27 to S31) confirmed the formation of photonic structures within 45 s.

Mixing core-shell microsphere suspensions with mediating monomers at room temperature enabled in situ absorption of monomers into the shells (Fig. 2C and fig. S32). This simple strategy eliminates complex pretreatment steps and allows direct coating of the colloidal suspensions onto PET substrates. Previously reported methods (*23*, *32*) for fabricating potentially large-scale photonic crystal involved an "extrusion + multiple calendering" process to uniformly incorporate additives with solid microspheres, analogous to rubber compounding, which produced films ~100 μm thick. By contrast, our coating method enhances production efficiency and reduces film thickness to 15 μm (fig. S33). Finite element analysis (FEA) simulations (Fig. 2D, figs. S34 to S36, and supplementary text 5) demonstrated that 15-μm-thick films experience greater strain under continuous bending, with minimal attenuation of shear forces, which enhanced internal ordering and improved film transparency, effectively avoiding structural disorder and opacity caused by uneven shear in thicker films. The fabricated films achieved lengths of up to 4000 m (Fig. 2E), with a width of 1.3 m (Fig. 2F). By varying the PS core sizes, CPC films with different colors can be obtained (Fig. 2G), all exhibiting well-ordered photonic structure and excellent optical properties (Fig. 2H and figs. S37 to S39), along with mechanochromic characteristics (fig. S40). Taking the blue 3D CPC film as an example, it exhibits the PBG intensity of 63%, 21 nm FWHM, and an average transmittance that exceeds 90% outside the PBG.

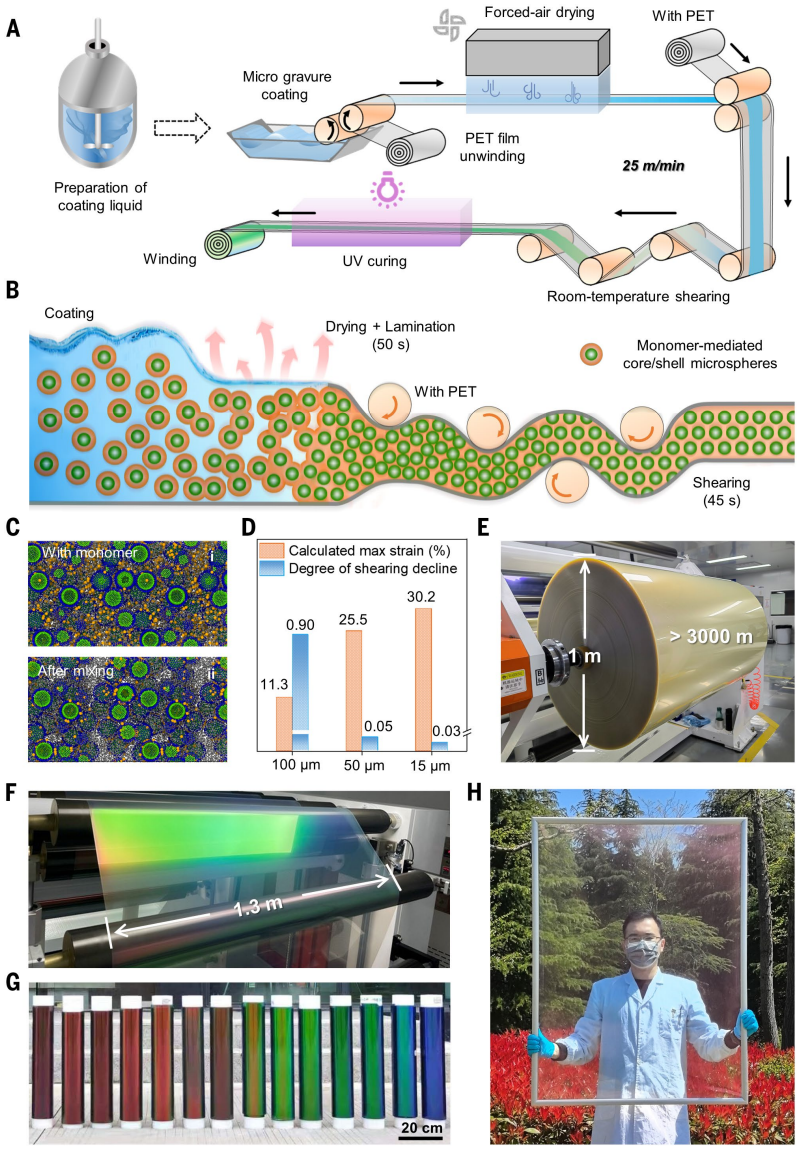

Fig. 2. Room-temperature high-throughput colloidal engineering for industrial-scale 3D CPC films. (**A**) Schematic illustration of industrial-scale continuous manufacture line. (**B**) Scheme of the microsphere arrangement during continuous manufacture. (**C**) The simulation of the process of mixing core (green)–shell (blue) microsphere suspensions with mediating monomers. (i) The beginning state of the core-shell microsphere suspensions with monomers (orange). (ii) The state after mild stirring. The gray beads indicate water. (**D**) Calculated max strain and degree of shearing decline of CPC film with different thickness from simulated bending process. (**E**) Continuous production of CPC film. (**F**) Photograph of the sandwiched CPC film during rolling up. (**G**) Rolls of photonic films with different colors (CPC–black base composite). (**H**) Outdoor demonstration of the transparency of a 1.3-m-wide red CPC film under indirect sunlight.

Mechanical properties of the 3D colloidal structural color films

The mediating monomers not only enabled the rapid assembly of colloidal particles but also polymerized within the matrix to form a dual network, enhancing the mechanical robustness of the CPC films. This process follows a broadly applicable physical pathway underpinned by supramolecular chemical design for nonequilibrium assembly (fig. S41). DEGDMA, containing two double bonds, acts as a covalent cross-linking agent, while the carbonyl and hydroxyl groups of 4-HBA and DEGDMA maintain their hydrogen bonds, yielding a noncovalent network within the shell. Compared with a single covalent cross-linked network (fig. S42), hydrogen bonds serve as sacrificial bonds (Fig. 3A, i), improving the elasticity and toughness of the CPC films (fig. S43). Stress-strain tests showed that a dual-network strategy increases both the elongation at break (Fig. 3B) and the tensile strength (Fig. 3C), with improvements exceeding twofold. For practical applications, the CPC films can be further reinforced by compounding with thermoplastic polyurethane film (TPU) to enhance mechanical performance (figs. S44 and S45). The dynamic dissociation and reformation of hydrogen bonds between polymer chains in the shell effectively endows the CPC film with self-healing capability (Fig. 3A, ii). The self-healing rate of the photonic film at room temperature is remarkably fast, and stress-strain tests confirmed complete recovery in ~1 min (Fig. 3D). The self-healing process is simple and requires only bringing two pieces of CPC film into contact at room temperature (Fig. 3E and supplementary text 6). FESEM cross-sectional images show that stable healing was achieved with no visible interfaces (fig. S46). Published fabrication techniques (fig. S47) (*24*, *33*–*38*) have produced CPC materials with excellent mechanical properties; however, they required tedious processing steps. By contrast, existing large-scale fabrication methods can yield films with good optical properties but generally lack mechanical strength, toughness, and elasticity. The industrial-scale 3D CPC films we report here combine both outstanding mechanical properties (>0.5 MPa) and excellent optical performance, offering an aspect ratio improved by at least three orders of magnitude (2.7×10^8) (fig. S47) compared with previous large-scale CPC films (*32*). The monomer-mediated colloidal assembly strategy developed in this study combines high-throughput assembly capability (25 m/min) with substantial advantages: (i) room-temperature process, (ii) continuous fabrication and speed, (iii) industrial-scale production, and (iv) excellent optical and mechanical properties, all of which overcome specific limitations of previously published methods (fig. S48, supplementary text 7, and table S2) (*21*, *23*, *32*, *39*–*42*).

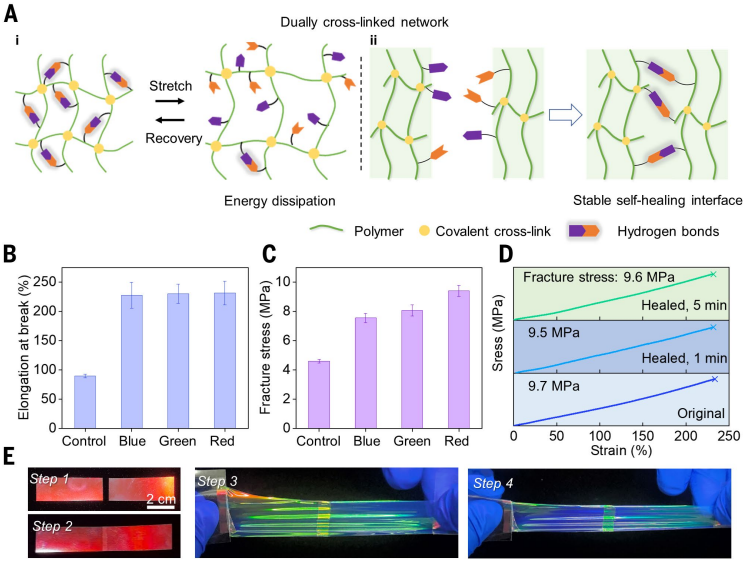

Fig. 3. Mechanical properties of industrial-scale 3D CPC structural color film. (**A**) Schematic demonstrating the matrix network variations of CPC film with dually cross-linked networks (i) during stretching and (ii) the function of hydrogen bonds in facilitating film self-healing. (**B**) Elongation at break and (**C**) fracture stress of CPC films with singly cross-linked network (control) and dually cross-linked network ($n = 3$ samples; error bars indicate mean ± SD). (**D**) Stress-strain curves of the original and self-healed CPC film with different healing times at 25°C. (**E**) Self-healing effect of CPC film at room temperature.

Application potentials of the colloidal structural color films

Conventional photovoltaic (PV) panels, which are typically black or dark blue, exhibit monotonous colors and limited aesthetic appeal. Although existing colored PV technologies offer improved aesthetic, they generally suffer from reduced power-conversion efficiencies. The self-supporting photonic crystal films exhibit vivid structural color, narrow reflection bandwidths, and excellent optical transparency outside the PBG, minimizing photon losses while providing a striking visual appearance. As a proof of principle, a small commercial PV panel was covered with a 15-μm-thick surface-patterned CPC film (Fig. 4A). External quantum efficiency (EQE) measurements of the PV panel with CPC film revealed only slight attenuation of incident photons within the PBG. Moreover, current-voltage and EQE characterization showed that introduction of the CPC film had negligible impact on short-circuit current density (J_{sc}), open-circuit voltage (V_{oc}), and fill factor (FF) (Fig. 4B and fig. S49). The decorated PV panel maintained 93 to 98% of the original power conversion efficiency (PCE). Additionally, our fabricated films retained excellent color saturation under continuous UV irradiation compared with that of pigment-based colored films, demonstrating superior color stability (figs. S50 to S52). The CPC films can be granulated at low temperature and subsequently embedded into ethylene-vinyl acetate (EVA) encapsulants to enhance their stability, generating colorful effects while providing a facile route for fabricating large-scale colored photovoltaic devices (Fig. 4C).

The fabricated 3D photonic crystal films also exhibit excellent mechanical characteristics, making them highly sensitive to external mechanical stimuli. For example, kinesio taping is a widely used technique in the clinical rehabilitation of muscle injuries, in which carefully monitored stretching can aid the recovery process. Whereas conventional tapes are monochromatic without any quantitative or visual feedback, we developed a kinesio tape (Fig. 4D) that exhibits distinct color changes under different strain (Fig. 4E), enabling a correlation between strain and perceived color (Fig. 4F and fig. S53). During use, the tape can be stretched to a specific target color corresponding to a desired strain, allowing for intuitive and precise control of applied stress, improving both therapeutic efficacy and user experience. Furthermore, integrating patterned CPC films into sports attire enables real-time visual feedback on body movements through strain-induced structural color changes (fig. S54). The presence of hydroxyl and carboxyl groups within the CPC film enhances its hydrophilicity (Fig. 4G), resulting in distinct color variations (Fig. 4H and supplementary text 8).

Conclusions

We have established a straightforward monomer-mediated formulation and processing window for colloidal assembly that enables rapid colloidal ordering within 10 s at room temperature. This result arises from added monomers, which effectively weaken interparticle interactions, modulate the viscoelasticity of the system, and bias the assembly pathway under shear. A range of common styrene and acrylate-based monomers are able to mediate this process, and subsequent polymerization enables macroscopic function to be imparted through supramolecular chemical design. Building on this principle, we developed an industrial-scale assembly platform capable of producing CPC films at room temperature with dimensions of up to 4000 m in

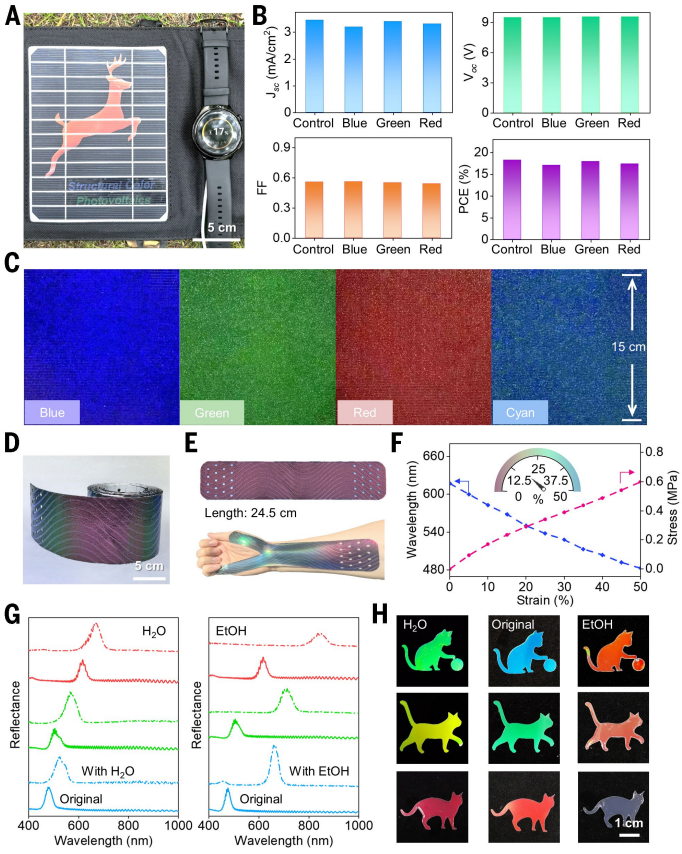

Fig. 4. Applications of colloidal structural color films. (**A**) Photovoltaic (PV) panel with surface CPC patterns. (**B**) Influence of blue, green, and red photonic crystal films on short-circuit current density (J_{sc}), open-circuit voltage (V_{oc}), fill factor (FF), and power conversion efficiency (PCE) of commercial PV panels. (**C**) Structural color PV panels. (**D**) Kinesio tape with CPC film as surface layer. (**E**) Structural color kinesio tapes in the original state and under different tensile strains. (**F**) Reflection peak positions and tensile stress of structural color kinesio tapes under different strains. (**G**) Reflection spectra of films upon exposure to water and ethanol. (**H**) Corresponding photographs, illustrating color changes.

length, 1.3 m in width, and 15 μm in thickness at a speed of 25 m/min. We demonstrated a range of advanced applications in photonics, sensing, and soft-matter engineering while laying the foundation for rapid assembly of anisotropic and hierarchically structured particles with precise control on an industrial scale.

REFERENCES AND NOTES

1. D. MacKinnon, M. Godzina, C. R. Becer, *Prog. Polym. Sci.* **165**, 101967 (2025).
2. J. S. Du, Y. Bae, J. J. De Yoreo, *Nat. Rev. Mater.* **9**, 229–248 (2024).
3. J. Li, F. L. Deepak, *Chem. Rev.* **122**, 16911–16982 (2022).
4. M. Ye *et al.*, *ACS Nano* **19**, 34847–34857 (2025).
5. C. Liang *et al.*, *Nat. Mater.* **24**, 599–606 (2025).
6. G. Amadei *et al.*, *Nature* **610**, 143–153 (2022).
7. M. He *et al.*, *Nature* **585**, 524–529 (2020).
8. V. N. Manoharan, *Science* **349**, 1253751 (2015).
9. S. Whitelam, R. L. Jack, *Annu. Rev. Phys. Chem.* **66**, 143–163 (2015).
10. C. Yi *et al.*, *Science* **369**, 1369–1374 (2020).
11. N. Kröger, R. Deutzmann, M. Sumper, *Science* **286**, 1129–1132 (1999).
12. F. Vollrath, D. P. Knight, *Nature* **410**, 541–548 (2001).
13. F. U. Hartl, A. Bracher, M. Hayer-Hartl, *Nature* **475**, 324–332 (2011).
14. Y. Sun *et al.*, *Nat. Chem.* **14**, 274–283 (2022).
15. Z. Cai *et al.*, *Chem. Soc. Rev.* **50**, 5898–5951 (2021).
16. J. E. S. V. Hoeven, A. V. Shneidman, N. J. Nicolas, J. Aizenberg, *Acc. Chem. Res.* **55**, 1809–1820 (2022).
17. F. Lu *et al.*, *Nat. Mater.* **24**, 785–793 (2025).
18. Y. Zhang *et al.*, *Nat. Commun.* **13**, 7095 (2022).
19. D. Wang *et al.*, *Nat. Phys.* **17**, 128–134 (2021).
20. W. Li, C. Zhang, Y. Wang, *Adv. Colloid Interface Sci.* **333**, 103286 (2024).
21. X. Wang *et al.*, *Chem. Eng. J.* **483**, 149053 (2024).
22. M. Kim, J. B. Kim, S. H. Kim, *Microsyst. Nanoeng.* **10**, 21 (2024).
23. Q. Zhao *et al.*, *Nat. Commun.* **7**, 11661 (2016).
24. L. Siegwardt, M. Gallei, *Adv. Funct. Mater.* **33**, 2213099 (2023).
25. M. Li *et al.*, *Adv. Mater.* **34**, e2110488 (2022).
26. S. H. Yu, R. O'Reilly, L. Jiang, N. A. Kotov, *Acc. Chem. Res.* **55**, 1783–1784 (2022).
27. Z. Li, Q. Fan, Y. Yin, *Chem. Rev.* **122**, 4976–5067 (2022).
28. Q. Gao *et al.*, *Nat. Mater.* **20**, 1431–1439 (2021).
29. C. Du *et al.*, *Macromolecules* **54**, 4313–4325 (2021).
30. X. Yang *et al.*, *Nat. Commun.* **13**, 6654–6663 (2022).
31. J. Zhao *et al.*, *J. Am. Chem. Soc.* **144**, 872–882 (2022).
32. M. Li *et al.*, *Nat. Commun.* **15**, 1874 (2024).
33. Y. Guan, H. Li, S. Zhang, W. Niu, *Adv. Funct. Mater.* **33**, 2215055 (2023).
34. X. Wang *et al.*, *ACS Appl. Nano Mater.* **5**, 729–736 (2022).
35. P. Wu *et al.*, *Nanoscale* **11**, 20015–20023 (2019).
36. Y. Hu, C. Qi, D. Ma, D. Yang, S. Huang, *Nat. Commun.* **15**, 5643 (2024).
37. F. Gao *et al.*, *Adv. Opt. Mater.* **13**, 2402892 (2025).
38. X. Li *et al.*, *J. Am. Chem. Soc.* **147**, 4357–4364 (2025).
39. B. H. Miller, H. Liu, M. Kolle, *Nat. Mater.* **21**, 1014–1018 (2022).
40. B. E. Droguet *et al.*, *Nat. Mater.* **21**, 352–358 (2022).
41. L. D. C. de Castro, J. Lub, O. N. Oliveira Jr., A. P. H. J. Schenning, *Angew. Chem. Int. Ed.* **64**, e202413559 (2025).
42. H. Huang *et al.*, *Adv. Mater.* **35**, e2211117 (2023).

ACKNOWLEDGMENTS

We appreciate the fruitful discussions with S. Sarkar and K. Sokołowski (Department of Chemistry, University of Cambridge). We are grateful to Y. Yang (Laboratory of Advanced Materials, Fudan University) for valuable suggestions on the manuscript and to L. Zuo and Y. Wang (Department of Polymer Science and Engineering, Zhejiang University) for their support with photovoltaic measurements. We thank P. Tan (Department of Physics, Fudan University) for constructive discussions with him during revision. We are grateful to F. Tian, Z. Chen, and Z. Tian from our group in helping with characterization during revision. F.T. is the chief executive officer and a shareholder of Phomera Metamaterials, and we thank Phomera Metamaterials for providing access to industrial-scale equipment used in this work. We are grateful to time-resolved USAXS Beamline BL10U1 at SSRF (Shanghai Synchrotron Radiation Facility, China) for providing the beam time. **Funding:** C. Wang acknowledges financial support from the National Natural Science Foundation of China (grants 52131308 and 51721002), Ministry of Science and Technology (grant 2022YFA1203002), and Key Research and Development Project of Guangdong Province (grant 2020B010190003). O.A.S. acknowledges financial support from the Senior Visiting Scholarship of State Key Laboratory, Fudan University (project 2024FGJ02), ERC CoG grant CAM-RIG 726470, and EPSRC Programme Grant RaNT (EP/R020965/1). H.L. acknowledges financial support from Shanghai Sailing Program (project 24YF2702000). **Author contributions:** Conceptualization: O.A.S., C.W., H.L., J.A.M. Methodology: H.L., J.Y., O.A.S., C.W. Software: J.Y., W.L. Validation: H.L., J.Y., G.Z., F.T., O.A.S., C.W. Formal analysis: C.W., H.L., J.Y., G.Z., H.H., J.A.M. Investigation: H.L., G.Z., J.Y., L.C., R.L. Resources: F.T. Data curation: H.L., J.Y., L.C., R.L., C.W. Visualization: H.L., J.Y., H.H., O.A.S., C.W. Funding acquisition: C.W., O.A.S., H.L. Supervision: C.W., O.A.S. Writing – original draft: H.L., O.A.S. Writing – review & editing: O.A.S., C.W., H.L., J.A.M. Project administration: C.W., O.A.S. **Competing interests:** The authors declare that they have no competing interests. **Data, code, and materials availability:** All data are available in the main text or the supplementary materials. All chemicals used in this study were obtained from commercial sources and used as received unless otherwise stated. Information on material sources and synthesis procedures is provided in the supplementary materials. This research was funded in whole or in part by EPSRC (EP/R020965/1), a cOAlition S organization. The author will make the Author Accepted Manuscript (AAM) version available under a CC BY public copyright license.

SUPPLEMENTARY MATERIALS

science.org/doi/10.1126/science.aed8723
Materials and Methods; Supplementary Text; Figs. S1 to S54; Tables S1 and S2; References (*43*–*59*); Movies S1 to S4

Submitted 21 November 2025; accepted 13 July 2026

10.1126/science.aed8723

Monomer-biased manufacture of industrial-scale colloidal photonic films

Huateng Li, Junying Yang, Guowei Zhao, Hanwen Huang, Lulu Chen, Ruoqi Lan, Feng Tian, Weihua Li, Jade A. McCune, Oren A. Scherman, and Changchun Wang

Science **393** (6815), . DOI: 10.1126/science.aed8723

Editor's summary

The self-assembly of ordered colloidal structures makes it possible to construct photonic structurally colored materials, but it is difficult to do so at large scales. Li *et al*. report an innovative monomer-mediated strategy for the rapid, industrial-scale fabrication of colloidal photonic crystal films. Introducing low-molecular-weight functional monomers biases the free energy landscape and assembly pathway, enabling rapid ordering under shear of colloidal particles under ambient and template-free conditions. The authors show disorder-to-order transformation of colloidal aggregates into photonic crystal films up to 4000 meters in length under ambient conditions without templates within 10 seconds. —Marc S. Lavine

Science (ISSN 1095-9203) is published by the American Association for the Advancement of Science. 1200 New York Avenue NW, Washington, DC 20005. The title *Science* is a registered trademark of AAAS.